Geol. Mag. **147** (*6*), *2010, pp. 844–859. © Cambridge University Press 2010*
doi:10.1017/S0016756810000373

Contrasting Middle Jurassic and Early Cretaceous mafic intrusive rocks from western Liaoning, North China craton: petrogenesis and tectonic implications

XIAOHUI ZHANG*†, HONGFU ZHANG*, NENG JIANG* & SIMON A. WILDE‡

*State Key Laboratory of Lithospheric Evolution, Institute of Geology and Geophysics, Chinese Academy of Sciences, Beijing 100029, China
‡Department of Applied Geology, Curtin University of Technology, Perth, WA 6845, Australia

(*Received* 1 September 2009; *accepted* 23 March 2010; *first published online* 7 May 2010)

Abstract – Zircon U–Pb dating, whole-rock major oxide, trace element and Sr–Nd isotopic data are presented for the Late Mesozoic mafic intrusive rocks from Yiwulüshan of western Liaoning along the eastern segment of the Yanshan belt, North China craton, with two episodes of magmatism documented. Middle Jurassic hornblende-rich gabbros show enrichment of large ion lithophile elements and light REE, and prominent depletion in high field strength elements, and possess moderately enriched isotopic compositions with $(^{87}Sr/^{86}Sr)_i$ ranging from 0.7056 to 0.7065 and $\varepsilon_{Nd}(t)$ from −5.0 to −7.1. These features suggest that the gabbros were derived from an amphibole-bearing harzburgitic lithospheric mantle source metasomatized recently by slab-derived fluids. By contrast, Early Cretaceous mafic dykes are gabbroic dioritic to dioritic in composition, with comparable trace element characteristics to continental crust and depleted isotopic signatures ($(^{87}Sr/^{86}Sr)_i = 0.7048–0.7055$, $\varepsilon_{Nd}(t) = 0$ to −3.0). They probably originated from partial melting of a relatively fertile asthenospheric mantle in the spinel stability field, with subsequent lower crustal assimilation and fractional crystallization. These two contrasting mafic intrusive suites, together with multiple Mesozoic mafic volcanic rocks from western Liaoning, documented a localized lithospheric thinning process, mainly through prolonged hydro-weakening or melt–rock interaction and triggered by gravitational collapse, possibly within an evolved post-collisional to within-plate extensional regime.

Keywords: mafic intrusions, Late Mesozoic, petrogenesis, lithospheric thinning, North China craton.

1. Introduction

As insightful compositional and thermal probes of their mantle sources and indicators of intracontinental tectonic regimes, continental mafic magmatism of different ages can provide a temporal proxy for documenting mantle–crust interaction and chemical–thermal evolution of the deep continental lithosphere and underlying mantle beneath plate margins (e.g. Farmer, 2003). In general, such magmas can be divided into two main types in terms of their typical geochemical characteristics: one bearing subduction-related geochemical signatures and the other with OIB-type geochemical features. Generation of the former can usually result from: (1) subduction of oceanic lithosphere (Hawkesworth *et al.* 1993); (2) melting of metasomatically enriched subcontinental lithosphere with an inherited subduction signature (Turner *et al.* 1996; Zhang *et al.* 2003); or (3) extensive crustal contamination of MORB-like magmas (Turner *et al.* 1999). These magmas are commonly thought to reflect lithospheric response to rapid changes in upper mantle geometry, such as (1) lithospheric extension by orogenic collapse (Rey, Vanderhaeghe & Teyssier, 2001 and references therein); (2) roll-back and detachment of subducted oceanic lithosphere (Davies & von Blanckenburg, 1995); (3) convective thinning of subcontinental lithosphere (England & Houseman, 1989; Platt & England, 1993); or (4) delamination of subcontinental lithosphere (Kay & Kay, 1993).

As one of the oldest cratons, the North China craton has experienced one of the most complex histories of any geological terrane on the planet, including an Archaean–Palaeoproterozoic stage of initial continental root formation, an intervening Palaeozoic quiescent stage and a Mesozoic–Cenozoic stage of orogeny, loss of continental root and decratonization (Kusky, Windley & Zhai, 2007*a*). It is this Phanerozoic decratonization stage that distinguishes the North China craton from most other cratons in the world. The typical mantle and crustal expressions of this distinctive stage are best manifested in the Yanshan belt, an intra-continental orogen that strikes east–west through the northern margin of the North China craton. They include marked compositional changes of the lithospheric mantle from a cold, thick and refractory Palaeozoic lithosphere to a hot, thin and fertile Cenozoic lithosphere, widespread Mesozoic magmatism, and the development of a series of Early Cretaceous metamorphic core complexes and rifted basins (Wu *et al.* 2008 and references therein).

The eastern segment of the Yanshan belt, western Liaoning province, experienced multiple episodes of magmatism during Mesozoic time. Recently, numerous

†Author for correspondence: zhangxh@mail.iggcas.ac.cn

studies of Mesozoic mafic–intermediate igneous rocks from this region have yielded abundant information about lithospheric thinning in the Yanshan belt (e.g. Fan *et al.* 2007; Gao *et al.* 2004, 2008; Guo *et al.* 2007; Shao *et al.* 2006; Wang *et al.* 2006; Yang & Li, 2008; Zhang *et al.* 2003; Zhang, 2007). However, these studies have been mostly confined to volcanic rocks. In this contribution, we present geochronological and geochemical investigations for contrasting Middle Jurassic and Early Cretaceous mafic intrusive rocks from the Yiwulüshan range of western Liaoning, where recent structural and geochronological investigations have documented an Early Cretaceous metamorphic core complex (Zhang, Wang & Ma, 2003; Darby *et al.* 2004). We aim to constrain the petrogenesis and characterize the evolution of the mantle sources of these rocks, thus probing possible mechanisms for the lithospheric thinning process of the Yanshan belt.

2. Geological background

The Yanshan belt, of the Beijing, northern Hebei and western Liaoning provinces, is located along the northern margin of the North China craton (Fig. 1a, b), which is bounded on the south by the Palaeozoic to Triassic Qinling–Dabie–Sulu orogenic belt (Meng & Zhang, 2000) and on the north by the Central Asian Orogenic Belt (Davis *et al.* 2001).

As shown by the presence of ≥ 3.6 Ga crustal remnants exposed at the surface or in lower crustal xenoliths (Liu *et al.* 1992; Zheng *et al.* 2004), the North China craton is regarded as one of the world's oldest cratons. It consists of two Archaean continental blocks, the Eastern Block and the Western Block, which are separated by the Proterozoic Trans-North China orogenic belt (Fig. 1a; Zhao *et al.* 2001). The basement of the North China craton is composed of amphibolite- to granulite-facies Archaean grey tonalitic gneisses and greenstones, Palaeoproterozoic khondalites and an overlying unmetamorphosed sedimentary cover from Mesoproterozoic onwards (Zhao *et al.* 2001; Kusky, Windley & Zhai, 2007*a*). It is widely believed that the Eastern and Western blocks developed independently from the late Archaean to early Palaeoproterozoic and collided to form a coherent craton at *c.* 1.85 Ga (Zhao *et al.* 2001).

Unlike other Archaean cratons, the North China craton has experienced widespread tectonothermal reactivation since Palaeozoic time, mainly due to the compound influences of circum-cratonic orogenic belts. To the north of the craton, the generally EW-trending Central Asian Orogenic Belt mainly consists of island arcs, ophiolites, oceanic islands, accretionary wedges, oceanic plateaux and microcontinents comparable to that of circum-Pacific Mesozoic–Cenozoic accretionary orogens (Xiao *et al.* 2003; Windley *et al.* 2007). The Solonker suture marks the closure of the palaeo-Asian ocean and the collision between the North China craton and Mongolian composite terranes during Early Permian time (Zhang *et al.* 2008*a*). Amalgamation of these blocks resulted in a unified North China–Mongolian plate (Davis *et al.* 2001).

From early Mesozoic time on, the Yanshan belt experienced multiple intracontinental tectono-magmatic events, mainly in response to continuing continental contraction along the northern and southern margins of the craton and the subduction along its eastern margin. At least two episodes of contractile tectonism are manifested by regional Jurassic unconformities (at *c.* 180 and 160 Ma) and cross-cutting relationships (Davis *et al.* 2001). Each of these contractional deformation events was followed by several episodes of volcanism, granitoid emplacement and terrestrial deposition. In Early Cretaceous time, the orogenic fabric of the belt was overprinted by widespread extensional signatures, including a series of metamorphic core complexes (Davies *et al.* 2001) and rift basins (Cope & Graham, 2007).

Western Liaoning province witnessed tectono-magmatic events consistent with the Yanshan belt during late Mesozoic time, such as multiple episodes of volcanism (Zhang *et al.* 2003; Gao *et al.* 2004, 2008; Wang *et al.* 2006; Yang & Li, 2008) and plutonism (Liu *et al.* 2002; Wu *et al.* 2006; Zhang *et al.* 2008*b*), and an Early Cretaceous extensional infrastructure (that is, the Waziyu metamorphic core complex in the Yiwulüshan range: Zhang, Wang & Ma, 2003; Darby *et al.* 2004).

According to a recent age data compilation by Wu *et al.* (2006) and other geochronological studies (e.g. Luo *et al.* 2001), Mesozoic intrusions from Western Liaoning appear to occur in four episodes (Fig. 1c). The first episode is of rare Triassic dioritic magmatism (221 ± 2 Ma); the second and third episodes are of voluminous Middle–Late Jurassic granitic plutonism represented by the Jianchang (175–190 Ma) and Yiwulüshan batholiths (170–155 Ma); and the fourth episode is of scattered Early Cretaceous intrusions (e.g. Shishan pluton).

As shown in Figure 1d, the Waziyu metamorphic core complex has an east–west dimension of 25 km and a north–south dimension of 60 km. The core consists predominantly of Mesozoic granitoid plutons and their country rocks, which include high- to medium-grade migmatitic orthogneiss and amphibolites of the Archaean crystalline basement. Plutons are granodioritic to granitic and grade outward into augen gneiss or migmatite. At structurally higher levels is the well-developed NNE-trending Waziyu ductile shear zone that, together with the related normal fault above it along the eastern margin of the Fuxin basin, constitutes the Waziyu detachment fault (Darby *et al.* 2004) and separates the core of the dome (the lower plate) from an upper plate of unmetamorphosed to low-grade metamorphosed middle–late Proterozoic Changcheng System and Mesozoic volcano-sedimentary rocks.

The Hengshan pluton, part of the Yiwulüshan batholith, is located 10 km to the east of Fuxin city and crops out over 140 km^2 (Fig. 2). It bears a diffuse intrusive contact with the surrounding Archaean gneisses and Proterozoic meta-sedimentary sequences

https://doi.org/10.1017/S0016756810000373 Published online by Cambridge University Press

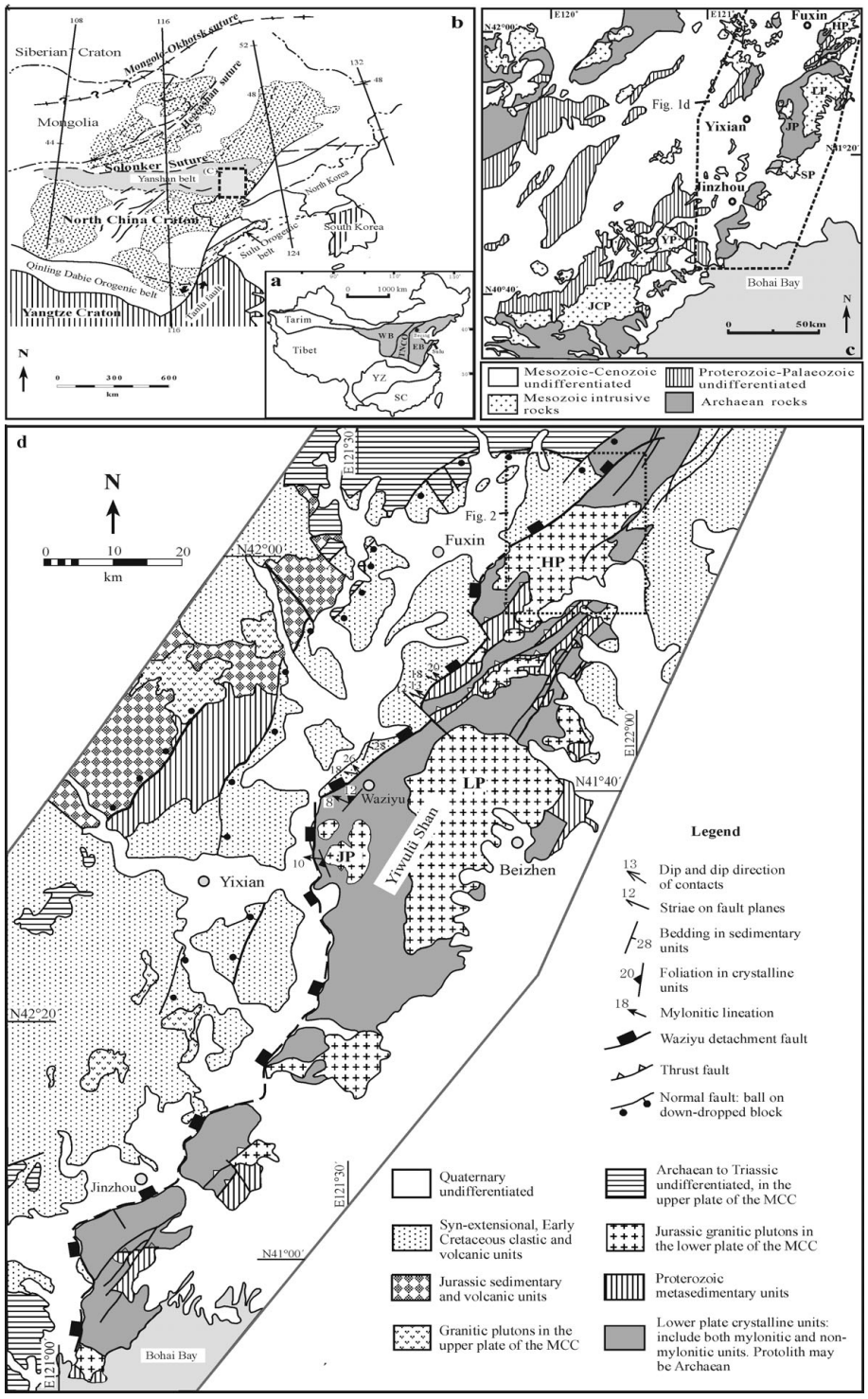

Figure 1. (a) Major tectonic divisions of China, where YZ and SC denote the Yangtze craton and South China orogen. Also shown are the subdivisions of the North China craton (Zhao *et al.* 2001), where EB, TNCO and WB denote the Eastern block, Trans-North China orogen and Western block, respectively. (b) Simplified geological map showing the major tectonic units of the North China craton and its surrounding areas, with the study area indicated by a rectangle (modified from Davis *et al.* 2001). Stippled fields denote the Mesozoic sedimentary basins. Dashed lines within the Mesozoic sedimentary basins are the trends of Jurassic–Cretaceous extensional faults. Between the Solonker Suture and the Mongolo-Okhotsk Suture is the Central Asian orogenic Belt (Şengör, Natal'in & Burtman, 1993). (c) Simplified geological map of western Liaoning province and distribution of the Mesozoic intrusive rocks (modified after Wu *et al.* 2006). (d) Simplified tectonic map of the Yiwulüshan, western Liaoning province (adopted from Darby *et al.* 2004), showing major structures and plutons. Pluton name abbreviations in (c) and (d): JCP – Jianchang pluton; JP – Jianlazi pluton; LP – Lüshan pluton; HP – Hengshan pluton, SP – Shishan pluton; YP – Yangjiazhangzi pluton; MCC – metamorphic core complex.

and is covered by Lower Cretaceous volcano-sedimentary strata of the Yixian Formation (Fig. 2). The pluton mainly consists of monzogranite, with subordinate granodiorite–monzonite and occasional gabbroic rocks. It is intruded by numerous late-stage mafic dykes. LA-ICPMS zircon U–Pb dating of two

https://doi.org/10.1017/S0016756810000373 Published online by Cambridge University Press

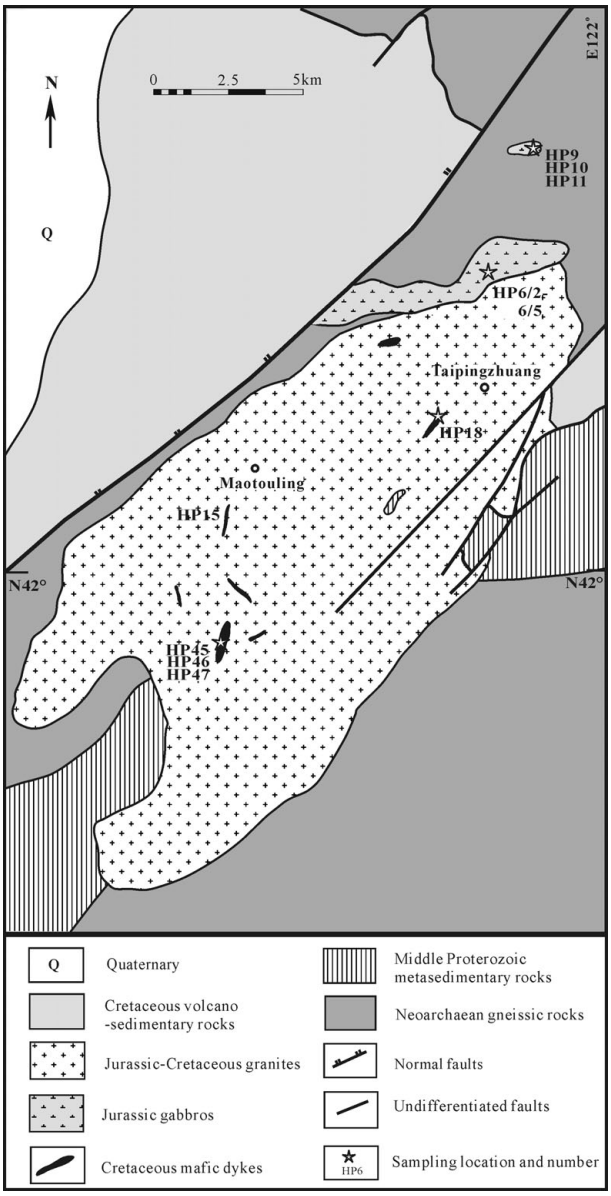

Figure 2. Sketch geological map of the Hengshan pluton (modified after LBGMR, 1998) in western Liaoning province.

monzogranite samples from different parts of the pluton yielded ages from 163 to 152 Ma, while those on the late-stage mafic dykes gave a weighted mean $^{206}Pb/^{238}U$ age of 125 ± 4 Ma (Wu *et al.* 2006). In addition, SHRIMP zircon U–Pb dating on the mafic dykes from the neighbouring Paishanlou gold deposit resulted in ages of 124–126 Ma (Luo *et al.* 2001; Zhang *et al.* 2005).

3. Petrography

The gabbroic rocks occur as small elongate epizonal bodies of the Hengshan pluton or as dykes intruding the Archaean gneisses (Fig. 2). They are fine- to medium-grained rocks with intergranular textures. Typical samples mainly consist of plagioclase (35–60 %), hornblende (25–50 %), pyroxene (0–5 %) and biotite (0–5 %) with minor amounts of alkali feldspar and quartz. Accessory phases include magnetite, zircon and apatite. Hornblende mainly occurs as subhedral to euhedral phenocrysts and is locally altered to chlorite. All hornblendes belong to the calcic group ($Ca+Na \geq 1$ and $Na < 0.5$), according to the classification of Leake *et al.* (1997) and can be classified as magnesiohastingsite and magnesiohornblende. Plagioclase is mainly subhedral in shape and 2–4.5 mm in size.

The late-stage mafic dykes in the Hengshan pluton are several to tens of metres in width and tens to several hundred metres in length. They commonly have a gabbroic dioritic to dioritic composition, with a fine-grained porphyritic texture. The main minerals are plagioclase (40–50 %), hornblende (25–35 %), biotite (10–15 %), K-feldspar (5 %), and minor quartz and clinopyroxene. Accessory phases include magnetite, ilmenite, zircon and apatite. The phenocrysts consist mainly of euhedral plagioclase and subhedral hornblende, with a size of 2–3.5 mm. The groundmass is similar in mineral assemblage to that of the phenocrysts but has a higher population of quartz, with a size of 0.2–1.5 mm.

4. Analytical methods

Zircon grains, together with standard CZ3, were cast in an epoxy mount, which was then polished to section the crystals in half for analysis. Cathodoluminescence images were obtained for zircons prior to analyses, using a JXA-8100 microprobe at the Institute of Geology and Geophysics, Chinese Academy of Sciences (IGGCAS), to reveal their internal structures. Measurements of U, Th and Pb were conducted using the SHRIMP II (sensitive high-resolution ion-microprobe) at Curtin University of Technology under standard operating conditions (6-scan cycle, 2 nA primary O_2^- beam, mass resolution ~5000), following analytical procedures as described by Williams (1998). Data were processed using the SQUID (1.02) and ISOPLOT (Ludwig, 2001) programs. Corrections of Pb/U ratios were made by normalization to zircon standard CZ3 ($^{206}Pb/^{238}Pb = 0.0914$, corresponding to an age of 564 Ma). The data were corrected for common lead using the measured ^{204}Pb. Individual analyses are reported with 1σ uncertainties, while weighted mean ages are reported at the 2σ confidence level.

For geochemical and isotopic analyses, samples were ground in an agate mill to ~200 mesh. Major oxides were analysed with a Phillips PW 2400 X-Ray fluorescence spectrometer (XRF) at the IGGCAS. Trace element abundances were obtained on a VG-PQII ICP-MS also at the IGGCAS. Samples were dissolved in distilled $HF+HNO_3$ in 15 ml high-pressure Teflon® bombs at 120 °C for 6 days, dried and then diluted to 50 ml for analysis. A blank solution was prepared and the total procedural blank was < 50 ng for all trace elements. Indium was used as an internal standard to correct for matrix effects and instrument drift. Precision for all trace elements is estimated to be 5 % and accuracy is better than 5 % for most elements by analyses of the GSR-3 standard.

https://doi.org/10.1017/S0016756810000373 Published online by Cambridge University Press

Table 1. SHRIMP U–Pb isotopic data for zircons from the Hengshan gabbros (sample HP9)

Spot no.	U (ppm)	Th (ppm)	Th/U	Pb(ppm)	Isotopic ratios						Age (Ma)
					$^{207}Pb/^{206}Pb$	1σ	$^{206}Pb/^{238}U$	1σ	$^{207}Pb/^{235}U$	1σ	$^{206}Pb/^{238}U \pm 1\sigma$
HP9–1	151	174	1.19	3.40	0.0547	0.0011	0.0263	0.0002	0.20	0.01	167 ± 3
HP9–2	304	262	0.89	7.0	0.0496	0.0006	0.0265	0.0001	0.18	0.06	169 ± 2
HP9–3	263	263	1.21	5.0	0.0493	0.0008	0.0259	0.0002	0.18	0.08	165 ± 2
HP9–5	783	1112	1.47	18.6	0.0515	0.0005	0.0273	0.0001	0.19	0.05	174 ± 2
HP9–7	238	269	1.17	5.6	0.0442	0.0015	0.0264	0.0002	0.16	0.01	168 ± 3
HP9–8	115	146	1.31	2.6	0.0576	0.0020	0.0258	0.0002	0.21	0.02	164 ± 3
HP9–9	259	393	1.57	5.9	0.0518	0.0006	0.0265	0.0001	0.19	0.06	168 ± 2
HP9–10	66	41	0.64	1.5	0.0218	0.0062	0.0253	0.0002	0.08	0.01	161 ± 4
HP9–11	1445	1557	1.11	33.2	0.0513	0.0002	0.0267	0.0001	0.19	0.02	170 ± 2

Sr and Nd isotopic compositions were measured on a Finnigan Mat 262 thermal ionization mass spectrometer at the IGGCAS, following the procedure as described in Zhang *et al.* (2008*a*). Procedural blanks were < 100 pg for Sm and Nd and < 500 pg for Rb and Sr. $^{143}Nd/^{144}Nd$ was corrected for mass fractionation by normalization to $^{146}Nd/^{144}Nd = 0.7219$, and $^{87}Sr/^{86}Sr$ ratios were normalized to $^{86}Sr/^{88}Sr = 0.1194$. The measured values for the BCR-2 Nd standard and NBS-987 Sr standard were $^{143}Nd/^{144}Nd = 0.512613 \pm 0.000012$ (2σ, n = 3) and $^{87}Sr/^{86}Sr = 0.710251 \pm 0.000011$ (2σ, n = 5) during the period of data acquisition.

5. Analytical results

5.a. Geochronology

Sample HP9 was collected from the gabbro unit of the Hengshan pluton and the results of SHRIMP zircon U–Pb analysis are listed in Table 1. Zircons from this sample are mostly clear, subhedral columnar crystals, with a length range from 60 to 120 μm and length to width ratios between 2:1 and 3:1 (Fig. 3a). In cathodoluminescence images, they typically show low, homogeneous luminescence and occasionally display oscillatory zoning (Fig. 3a). Nine analyses from this sample were conducted on nine grains during a single analytical session. Measured U concentrations vary from 66 to 151 ppm, and Th from 41 to 1557 ppm. All analyses have Th/U ratios of 0.64–1.57 and yield a weighted mean $^{206}Pb/^{238}U$ age of 167 ± 6 Ma with an MSWD of 0.85 (Fig. 3b). We interpret this as the emplacement age of the Hengshan gabbros.

5.b. Major and trace elements

Major and trace element analyses are presented in Table 2. Samples from the Hengshan gabbros are mafic in composition (SiO_2 43.2–49.4 %), with high abundances of total Fe_2O_3 (9.6–14.2 %), Al_2O_3 (18.2–19.9 %) and CaO (8.4–11.0 %), low contents of TiO_2 (0.6–1.7 %), P_2O_5 (0.08–0.47 %) and K_2O (0.5–1.1 %), and moderate MgO (4.0–6.9 %). In the total alkali versus silica plot (Le Maitre, 2002) (Fig. 4a), the samples mainly plot in the field of gabbro. They also exhibit a transitional character between low-K tholeiitic and medium-K calc-alkaline (Fig. 4b). As for trace

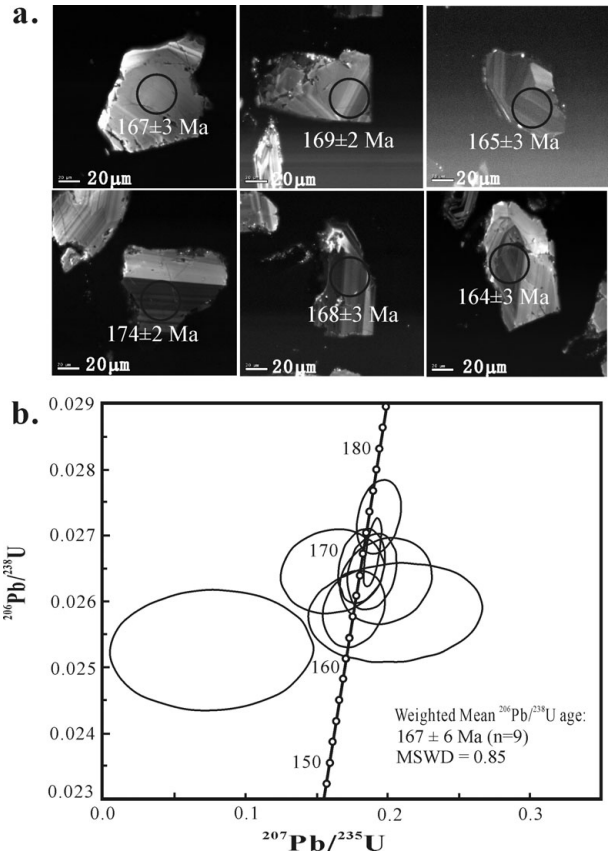

Figure 3. (a) Cathodoluminescence (CL) images of dated zircons and (b) U–Pb zircon concordia diagrams for the Hengshan gabbros.

elements, they have total REE contents ranging from 87.8 to 166 ppm, and are moderately enriched in LREE ($La_N/Yb_N = 4.3–9.1$) with slight negative or positive Eu anomalies ($Eu/Eu^* = 0.84–1.13$; Table 3) (Fig. 5a). In the primitive mantle-normalized spidergrams (Fig. 5b), they exhibit positive Rb, Ba and Sr anomalies, and negative Nb, Ta, Zr and Hf anomalies.

The mafic dykes are gabbroic dioritic to dioritic in composition (SiO_2 = 53.34–61.07 %). They show high contents of Al_2O_3 (15.7–17.7 %), CaO (4.77–6.93 %) and Na_2O (2.96–4.14 %), moderate contents of MgO (2.17–5.53 %) and K_2O (1.65–2.73 %), and low concentrations of TiO_2 (0.87–1.16 %), Cr (16.2–89.4 ppm) and Ni (7.23–33.6 ppm). In the total alkali versus silica plot (Le Maitre, 2002) (Fig. 4a), the samples mainly plot in the field of gabbroic diorite and monzodiorite. They show a medium-K

https://doi.org/10.1017/S0016756810000373 Published online by Cambridge University Press

Table 2. Major and trace element data for the contrasting Middle Jurassic and Early Cretaceous mafic intrusive rocks from western Liaoning

	Middle Jurassic gabbros						
Sample	HP-6/2	HP-6/4	HP-6/5	HP-6/6	HP-9	HP-10	HP-11
SiO_2	42.86	44.31	49.44	43.84	44.1	43.18	46.93
TiO_2	1.84	1.77	1.01	1.89	1.81	1.84	1.40
Al_2O_3	18.15	19.00	19.27	18.71	19.71	19.93	21.15
TFe_2O_3	14.20	13.12	9.58	12.55	13.49	13.76	11.02
MnO	0.15	0.12	0.13	0.13	0.14	0.14	0.11
MgO	5.96	5.88	5.80	6.94	4.12	3.96	5.72
CaO	9.98	9.75	8.42	9.93	10.77	10.96	6.63
Na_2O	2.34	2.53	3.59	2.21	1.8	1.89	3.01
K_2O	0.98	0.98	0.53	1.08	0.82	0.83	0.82
P_2O_5	0.78	0.40	0.31	0.13	0.25	0.25	0.20
LOI	2.43	1.63	1.52	2.25	2.61	2.78	2.82
Total	99.67	99.50	99.60	99.66	99.62	99.52	99.81
Mg no.	45.4	47.0	54.5	52.3	37.7	36.3	50.7
Sc	25.9	25.2	18.7	32.9	22.9	23.6	22.7
V	323	284	208	365	319	338	287
Cr	12.5	7.99	125	35.7	4.99	5.77	9.34
Co	30.7	29.1	27.6	44.2	30.6	33.5	41.5
Ni	14.8	12.6	36.2	31.4	7.22	8.14	8.54
Ga	24.0	22.9	21.6	21.8	24.1	23.3	22.5
Rb	20.9	21.7	10.8	24.8	19.4	19.0	19.3
Sr	749	818	845	684	799	814	698
Y	30.6	23.3	14.2	22.4	19.8	21.1	23.8
Zr	70.7	65.3	51.3	63.5	58.0	61.9	67.6
Nb	6.28	5.93	4.70	5.99	5.21	5.78	6.54
Cs	0.36	1.58	0.51	1.51	0.58	0.58	0.35
Ba	291	399	240	288	259	270	366
Hf	2.55	2.24	1.72	2.26	1.99	2.16	2.41
Ta	0.37	0.37	0.27	0.36	0.56	0.41	0.38
Pb	4.31	5.14	5.49	5.19	5.01	5.37	4.05
Th	1.10	1.13	0.73	0.74	0.75	0.95	1.03
U	0.23	0.28	0.19	0.20	0.25	0.31	0.23
La	24.4	16.3	17.4	12.6	11.4	12.1	16.7
Ce	61.0	39.1	37.7	30.7	31.8	34.8	39.3
Pr	9.16	5.78	5.13	4.92	4.59	4.98	5.04
Nd	37.8	24.7	18.8	21.6	19.6	22.6	22.7
Sm	8.54	6.22	3.70	5.71	4.63	5.41	5.53
Eu	2.20	1.91	1.29	1.64	1.49	1.52	1.48
Gd	7.58	5.73	3.28	5.31	4.69	5.09	5.37
Tb	1.19	0.86	0.49	0.83	0.75	0.80	0.76
Dy	6.10	4.74	2.66	4.62	3.91	4.32	4.31
Ho	1.20	0.91	0.54	0.90	0.74	0.81	0.87
Er	3.03	2.32	1.39	2.23	2.05	2.28	2.31
Tm	0.41	0.31	0.20	0.311	0.26	0.29	0.34
Yb	2.63	1.94	1.38	1.92	1.68	2.01	1.94
Lu	0.35	0.26	0.20	0.27	0.24	0.29	0.28
La_N/Yb_N	6.66	6.05	9.07	4.72	4.86	4.30	6.16
Eu/Eu^*	0.84	0.98	1.13	0.91	0.98	0.89	0.84
	Early Cretaceous mafic dykes						
Sample	HP-15	HP-18	HP-45	HP-46	HP-47	LX08[1]	LX09[1]
SiO_2	54.23	54.16	53.68	53.43	61.07	60.41	53.34
TiO_2	1.06	1.04	1.16	1.18	0.87	0.91	0.86
Al_2O_3	17.22	17.43	17.68	17.62	16.84	17.18	15.73
TFe_2O_3	7.63	8.13	8.63	8.76	5.28	5.67	6.69
MnO	0.11	0.1	0.13	0.13	0.09	0.1	0.11
MgO	5.53	4.63	4.37	4.48	2.43	2.17	4.85
CaO	7.51	6.57	6.63	6.79	4.77	4.77	6.93
Na_2O	2.96	3.89	4.1	4.14	4.1	3.88	3.08
K_2O	1.75	1.77	1.73	1.65	2.14	2.73	1.86
P_2O_5	0.15	0.25	0.27	0.27	0.23	0.3	0.18
LOI	1.49	1.72	1.68	1.65	1.87	1.81	5.97
Total	99.64	99.69	100.06	100.1	99.7	99.93	99.6
Mg no.	58.9	53.0	50.1	50.3	47.7	43.1	58.9
Sc	8.41	13.4	15.4	14.5	7.83	5.99	6.39
V	177	162	167	175	103	107	157
Cr	43.1	22.8	67.5	81.9	27.4	16.2	89.4
Co	20.7		24.3	24.2	11.7	17.4	21.9
Ni	21.0	20.3	17.7	30.6	7.23	10.3	33.3
Ga	20.6	19.7	19.4	19.0	20.5	22.2	19.1
Rb	66.5	47.3	40.1	41.6	35.3	61.5	64.6
Sr	357	612	618	648	541	691	400

https://doi.org/10.1017/S0016756810000373 Published online by Cambridge University Press

Table 2. Continued

	Early Cretaceous mafic dykes						
Sample	HP-15	HP-18	HP-45	HP-46	HP-47	LX08[1]	LX09[1]
Y	12.0	18.1	18.4	18.7	12.9	9.33	12.4
Zr	72.1	125	120	113	158	160	73.6
Nb	1.84	7.56	7.37	7.32	8.86	2.63	1.37
Cs	1.49	1.44	1.48	1.3	1.05	1.50	1.52
Ba	378	408	412	356	511	780	274
Hf	2.29	3.46	3.54	3.38	4.41	4.40	2.34
Ta	0.18	0.88	0.68	1.02	0.85	0.09	0.08
Pb	7.05	7.82	7.49	8.04	11.3	11.4	7.1
Th	3.02	2.76	2.91	2.4	4.63	3.12	3.04
U	1.19	0.91	0.86	0.77	1.59	1.16	1.54
La	14.0	17.25	19.6	17.3	23.6	27.7	14.2
Ce	27.3	43.22	41.5	37.9	46.5	55.2	29.5
Pr	4.03	5.47	5.32	5.09	5.76	6.24	3.63
Nd	15.7	21.95	22.3	21.8	23.1	23.0	14.6
Sm	3.54	4.57	4.82	4.94	4.39	4.01	3.2
Eu	1.02	1.46	1.42	1.44	1.27	1.24	1.01
Gd	3.21	4.42	4.52	4.4	3.6	3.39	3.24
Tb	0.49	0.59	0.67	0.64	0.49	0.43	0.52
Dy	2.48	3.46	3.79	3.74	2.67	2.01	2.5
Ho	0.45	0.72	0.76	0.76	0.51	0.35	0.48
Er	1.27	1.89	2.06	2.06	1.36	1.01	1.37
Tm	0.18	0.25	0.29	0.29	0.19	0.13	0.2
Yb	1.17	1.65	1.84	1.76	1.15	0.81	1.22
Lu	0.18	0.22	0.28	0.25	0.17	0.12	0.16
La_N/Yb_N	8.6	7.5	7.66	7.04	14.7	24.5	8.4
Eu/Eu*	0.93	0.99	0.94	0.94	0.98	1.03	0.95

1. Data cited from Liu *et al.* (2002).

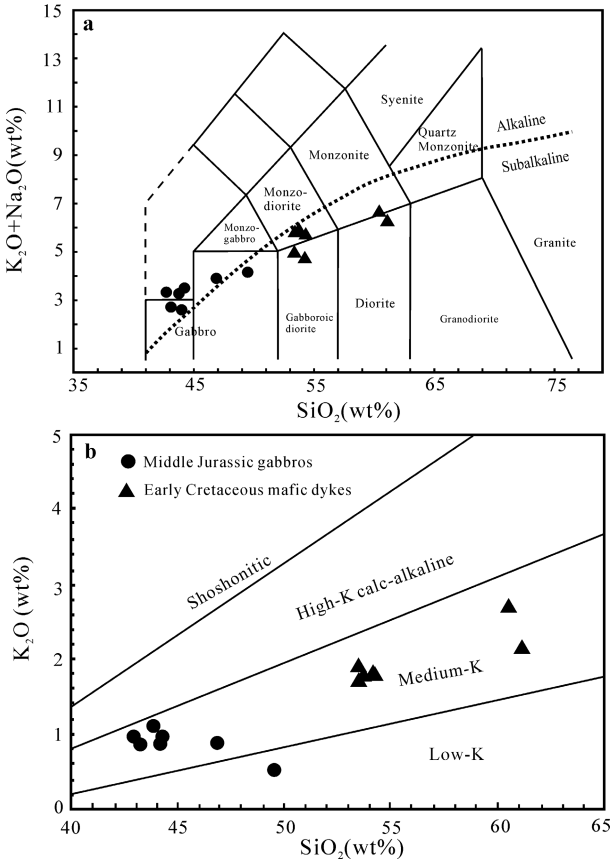

Figure 4. Plots (a) total alkali (Le Maitre, 2002) and (b) K_2O v. SiO_2 for the contrasting middle Jurassic and early Cretaceous mafic intrusive rocks from western Liaoning.

calc-alkaline character (Fig. 4b). In terms of trace elements, they are enriched in LREE (La_N/Yb_N = 7.04–24.5) and are relatively depleted in HREE with no negative Eu anomalies (Fig. 5c). In the primitive mantle-normalized spidergrams (Fig. 5d), they are moderately enriched in large ion lithophile elements (LILE) with positive Ba, Sr, Th and U anomalies, and are depleted in high field strength elements (HFSE) with pronounced negative Nb, Ta and Ti anomalies.

5.c. Whole rock Sr–Nd isotopes

The results of whole-rock Sr–Nd isotope analyses, together with the calculated initial Sr–Nd isotopic compositions, are presented in Table 3. Depleted mantle model ages T_{DM1} and T_{DM2} are computed by following the model of DePaolo (1981). As shown in a plot of $\varepsilon_{Nd}(t)$ versus $(^{87}Sr/^{86}Sr)_i$ (Fig. 6), the gabbros exhibit a narrow $(^{87}Sr/^{86}Sr)_i$ range from 0.7056 to 0.7065, relatively high $\varepsilon_{Nd}(t)$ values of −5.0 to −7.1 and model ages (T_{DM2}) of 1360 to 1526 Ma. Meanwhile, the mafic dykes have a narrow $(^{87}Sr/^{86}Sr)_i$ range from 0.7048 to 0.7055, zero to slightly negative $\varepsilon_{Nd}(t)$ values from 0 to −3.0 and younger model ages (T_{DM2}) of 921 to 1161 Ma.

6. Discussion

6.a. Petrogenesis

6.a.1. Middle Jurassic gabbros

The Middle Jurassic Hengshan gabbroic rocks, with their distinctive low silica contents (SiO_2 = 42.9–49.4 %) and higher concentrations of Fe_2O_3 (7.7–12.8 %) than those of any crustal materials (Rudnick & Gao, 2003) or crustally derived melts (e.g. Patiño

https://doi.org/10.1017/S0016756810000373 Published online by Cambridge University Press

Table 3. Rb–Sr and Sm–Nd isotopic compositions for the contrasting Middle Jurassic and Early Cretaceous mafic intrusive rocks from western Liaoning

Sample	Rb (ppm)	Sr (ppm)	$^{87}Rb/^{86}Sr$	$^{87}Sr/^{86}Sr$	2σ	$(^{87}Sr/^{86}Sr)_i$	Sm (ppm)	Nd (ppm)	$^{147}Sm/^{144}Nd$	$^{143}Nd/^{144}Nd$	2σ	ε_{Nd} (0)	ε_{Nd} (t)	T_{DM} (Ma)	T_{DM2} (Ma)
Hengshan pluton (t = 167 Ma)															
HP-6/4	20.7	885	0.0678	0.70664	13	0.70648	6.04	25.3	0.1444	0.512216	13	−8.2	−7.1	2047	1526
HP-6/5	10.8	908	0.0344	0.70606	13	0.70598	3.51	18.3	0.1162	0.512217	11	−8.2	−6.5	1456	1480
HP-6/6	24.3	801	0.0877	0.70621	12	0.70600	5.50	21.8	0.1524	0.512293	14	−6.7	−5.8	2123	1417
HP-9	17.8	821	0.0628	0.70576	8	0.70562	5.19	34.7	0.0906	0.512266	7	−7.3	−5.0	1094	1360
Mafic dykes (t = 125 Ma)															
HP-15	66.5	357	0.5396	0.70611	10	0.70489	3.54	15.7	0.1366	0.512519	9	−2.3	−1.4	1246	1028
HP-45	40.6	678	0.1743	0.70513	12	0.70482	4.84	22.6	0.1295	0.512581	12	−1.1	−0.0	1030	921
HP-46	38.7	700	0.1616	0.70515	13	0.70486	4.83	22.0	0.1329	0.512568	12	−1.4	−0.4	1097	945
HP-47	58.0	662	0.2554	0.70596	12	0.70547	4.64	24.1	0.1165	0.512419	12	−4.3	−3.0	1146	1161

Chondrite Uniform Reservoir (CHUR) values ($^{87}Rb/^{86}Sr = 0.0847$, $^{87}Sr/^{86}Sr = 0.7045$, $^{147}Sm/^{144}Nd = 0.1967$, $^{143}Nd/^{144}Nd = 0.512638$) are used for the calculation. $\lambda_{Rb} = 1.42\times10^{-11}$ year^{-1} (Steiger & Jäger, 1977); $\lambda_{SM} = 6.54\times10^{-12}$ year^{-1} (Lugmair & Marti, 1978).

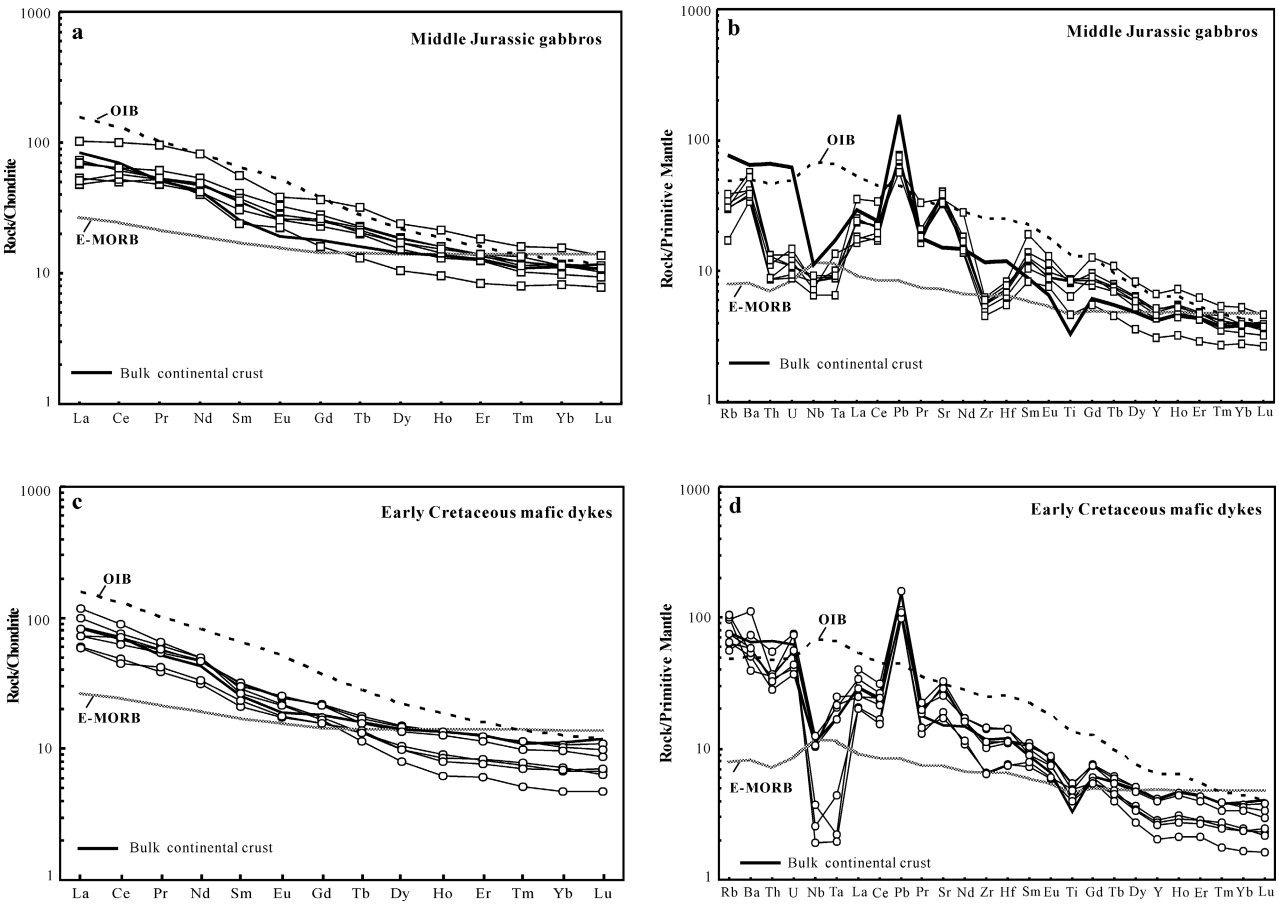

Figure 5. (a, c) Chondrite-normalized REE patterns, and (b, d) primitive mantle-normalized trace element spidergrams for the contrasting Middle Jurassic and Early Cretaceous intrusive rocks from western Liaoning. Normalization values are from Sun & McDonough (1989). The data for oceanic island basalt (OIB) and enriched mid-ocean ridge basalt (E-MORB) are also from Sun & McDonough (1989). Bulk continental crust compositions are from Rudnick & Gao (2003).

Douce & Beard, 1995; Patiño Douce, 1997), clearly argue for a mantle origin. On one hand, their hornblende-rich petrographic character is reminiscent of the high-level hornblende-rich mafic intrusions from the Mesozoic Sierra Nevada batholith (Sisson, Grove & Coleman, 1996) and the appinite suite from the late Caledonian granitoids within Europe (Fowler & Henney, 1996). As documented in these localities, such petrological features commonly indicate that their parental magma was rich in H_2O and arguably was derived from an enriched region of the mantle associated with subduction. On the other hand, the thick dyke occurrence of the Hengshan gabbros precludes a cumulate origin. This is consistent with the MgO, Cr and Ni contents in the gabbros, which are far below those expected for the rocks with a cumulate origin (MgO > 15 %, Cr > 2000 ppm, Ni > 300 ppm) (e.g. Roberts *et al.* 2000). Instead, their moderate Mg no. (40–59), low Cr (5–125 ppm) and Ni (13–31 ppm) concentrations indicate that they do not

https://doi.org/10.1017/S0016756810000373 Published online by Cambridge University Press

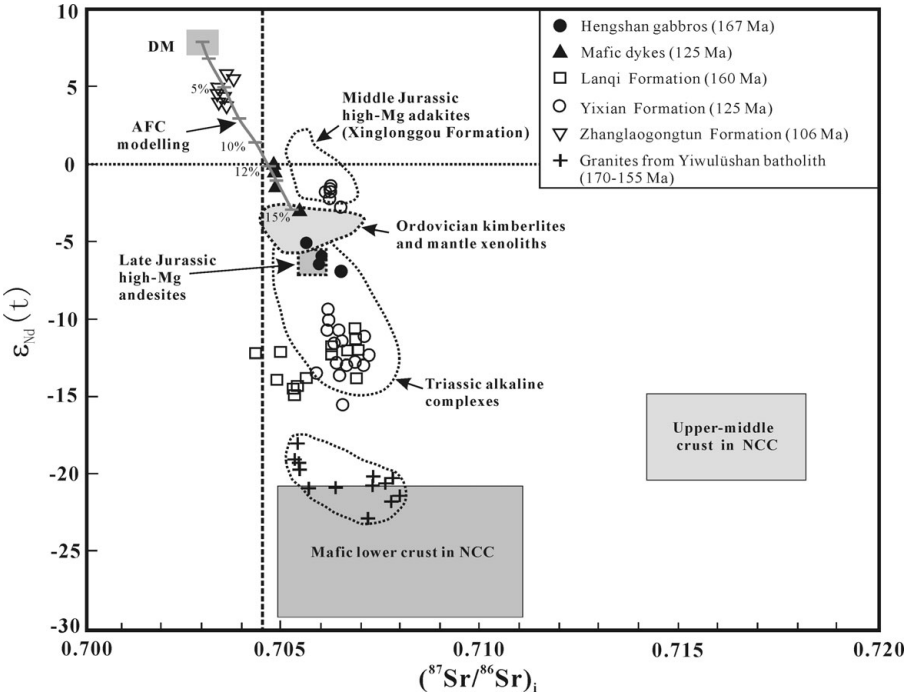

Figure 6. Plot of initial $\varepsilon_{Nd}(t)$ and $(^{87}Sr/^{86}Sr)_i$ for the contrasting Middle Jurassic and Early Cretaceous intrusive rocks from western Liaoning. Data sources: Lanqi formation – Yang & Li (2008); Xinglonggou formation – Gao *et al.* (2004); Yixian formation – Shao *et al.* (2006); Gao *et al.* (2008), Yang & Li (2008); late-Jurassic high-Mg andesite – Zhang *et al.* (2003); Zhanglaogongtun formation – Zhang *et al.* (2003); Yang & Li (2008); granites from Yiwulüshan batholith – Zhang *et al.* (2008b) and our unpublished data (online Appendix Table A1 at http://www.cambridge.org/journals/geo). Data (calculated at 160 Ma) for the Ordvician kimberlites and mantle xenoliths from the North China craton are from Yang *et al.* (2009) and Zhang (2009); for the Late Triassic alkaline intrusive rocks from Yan *et al.* (2000). Depleted mantle (DM) is from Zindler, Staudigel & Batiza (1984). Lower crust and upper–middle crust of the North China craton are from Jahn *et al.* (1999). The assimilation–fractional-crystallization (AFC) modelling parameters used for lower crust-derived melts of North China craton are Sr = 300 ppm, $^{87}Sr/^{86}Sr = 0.708$, Nd = 25 ppm, $\varepsilon_{Nd} = -25$ and Sr = 150 ppm, $^{87}Sr/^{86}Sr = 0.703$, Nd = 15 ppm, $\varepsilon_{Nd} = +8$ for depleted mantle derived melts.

represent primary magmas, but may have experienced some crystal fractionation, most likely of olivine and clinopyroxene, as reflected by the positive correlation between Cr and Ni contents (not shown).

In terms of trace elements, the Hengshan gabbros are characterized by selective enrichment of LILEs and light REE, and depletion in HFSEs (e.g. Nb, Ta and Ti), thus leading to high values of La/Nb (2.08–3.89), Ba/Nb (46–67), Zr/Nb ratios (~11) and low Ce/Pb (5.9–14.1). These values bear close resemblance to those of arc volcanic rocks worldwide (e.g. Stern, 2002). In general, such geochemical features can be attributed either to partial melting of an enriched mantle source that was previously spiked in LILE and LREE by slab-derived hydrous fluids or melts prior to magma generation, or to extensive crustal contamination of MORB-like magmas during magma ascent and emplacement. For the gabbros herein, their higher Sr abundance (684–845 ppm) than that of continental crust (Sr = 280–348 ppm: Rudnick & Gao, 2003) and distinct Sr–Nd isotopic compositions ($(^{87}Sr/^{86}Sr)_i = 0.7056–0.7065$, $\varepsilon_{Nd}(t) = -5.0$ to -7.1) from those of the lower crust of the North China craton exclude crustal contamination from having played any significant role in their petrogenesis.

Therefore, an enriched sub-continental lithospheric mantle source is implied for the Hengshan gabbros, as in the cases of their coeval or slightly older mafic volcanic counterparts from the Yanshan belt. Recent geochemical studies on the latter have documented a moderately enriched lithospheric mantle beneath the Yanshan belt during Jurassic time (Wang *et al.* 2007; Guo *et al.* 2007; Zhang *et al.* 2003; Zhang, 2007). More specifically, as constrained by Late Jurassic high-Mg andesites (Zhang *et al.* 2003) and primitive basaltic rocks (Zhou *et al.* 2001), the Jurassic lithospheric mantle beneath western Liaoning had an EM1 character ($(^{87}Sr/^{86}Sr)_i \approx 0.7060$; $\varepsilon_{Nd}(t) \approx -6.0$), slightly different from that of the Palaeozoic refractory lithospheric mantle beneath the North China craton as constrained by the Ordovician kimberlites and mantle xenoliths (Fig. 6) (Yang *et al.* 2009; Zhang, 2009).

Further information on this enriched lithospheric mantle can be inferred from the geochemical characteristics of the gabbros. First, the low Rb/Sr (0.01–0.04) and moderate Ba/Rb (13–22) ratios in the gabbros suggest an amphibole-bearing source (Furman & Graham, 1999). Second, the high Al_2O_3 contents in them require a high proportion of Al_2O_3-hosting minerals (such as garnet, spinel, clinopyroxene and orthopyroxene) in the mineral constituents of the mantle source, whereas the relatively high HREE abundances (Y > 14 ppm, Yb > 1.4 ppm) reflect a garnet-absent or garnet-poor source. With spinel

https://doi.org/10.1017/S0016756810000373 Published online by Cambridge University Press

commonly occurring as an accessory phase of the lithosphere, the dominant Al_2O_3-hosting phase in the mantle source should have been pyroxenes. Therefore, we argue that the parental magmas for the Hengshan gabbros could have been derived from partial melting of amphibole-bearing pyroxenite veins that resided in refractory lithospheric mantle beneath the Yanshan belt, possibly at a garnet-spinel transitional stability field with a depth of 70–80 km (Watson & McKenzie, 1991). Such a vein-rich mantle source may have been formed through multiple metasomatism events by the melts/fluids from subduction-related processes.

Different types of metasomatic agents (e.g. fluid, silicic or carbonatite melt) will yield distinctive trace element and isotopic compositions in metasomatized mantle (e.g. Menzies, 1987). In general, the Ba/La fractionation can only be reasonably achieved by elemental mobility in hydrous fluids (McCulloch & Gamble, 1991), whereas Th and LREE are thought to be less mobile in aqueous fluids than the LILEs (Pearce *et al.* 1999). As a result, these variables can serve as reliable indicators of potential melt or fluid contributions to magma source regions (Woodhead *et al.* 2001). For the Hengshan gabbros, Figure 7a clearly shows this contribution mainly comes from slab-derived fluids. Meanwhile, the high $(Hf/Sm)_{PM}$ and low $(Ta/La)_{PM}$ ratios in the gabbros also point to a fluid-related subduction metasomatism (Fig. 7b). This is consistent with the fluid-dominated enrichment process recorded by the Mesozoic mafic volcanic rocks throughout the Yanshan belt (Fan *et al.* 2007, Guo *et al.* 2007; Zhang, 2007).

6.a.2. *Early Cretaceous mafic dykes*

As shown above, the late-stage mafic dykes from the Hengshan pluton have distinct elemental and Sr–Nd isotopic compositions from the Middle Jurassic gabbros, thus precluding a common source and similar petrogenesis. Instead, they resemble the coeval olivine basalts from the bottom of the Yixian formation (Shao *et al.* 2006; Gao *et al.* 2008), with their high Mg no. (> 50) and comparable $\varepsilon_{Nd}(t)$ values (0 to −3). These basalts have been interpreted to contain a depleted mantle component ($\varepsilon_{Nd}(t) = +8$) (Shao *et al.* 2006; Gao *et al.* 2008). Another possible analogue is Late Triassic dolerite dykes from Eastern Liaoning (Yang *et al.* 2007), as indicated by their comparable incompatible trace element abundances and Sr–Nd isotopic compositions. The latter have been considered to be the product of high-degree partial melting of a relatively fertile asthenospheric mantle source in the spinel stability field, coupled with the subsequent upper crustal assimilation and crystal fractionation (Yang *et al.* 2007).

Strong crustal signatures are also evident in our mafic dykes. First, they display similar trace element patterns to bulk continental crust (Fig. 5c), with enrichment of LILEs and LREEs, and depletion of HFSEs. Second, they have comparable La_N/Yb_N (7–14.7), Ce/Pb

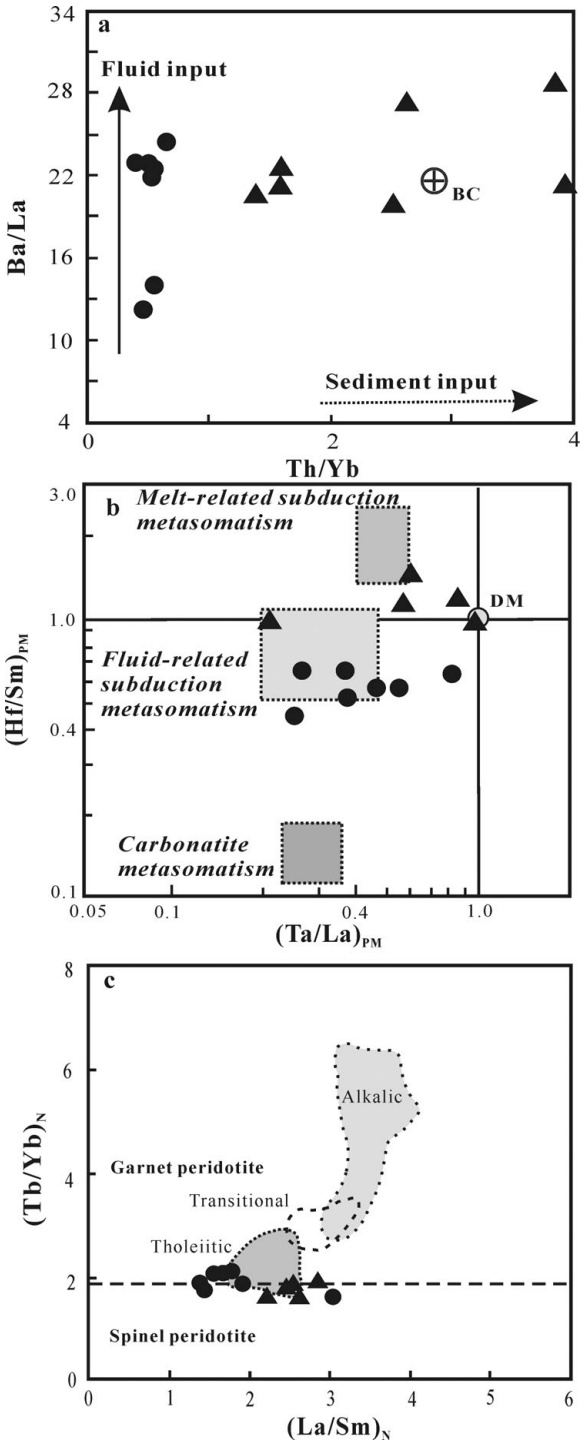

Figure 7. (a) Ba/La v. Th/Yb, (b) $(Ta/La)_{PM}$ v. $(Hf/Sm)_{PM}$ and (c) $(La/Sm)_N/(Tb/Yb)_N$ plots for the contrasting Middle Jurassic and Early Cretaceous intrusive rocks from western Liaoning. Sample symbols are the same as those in Figure 4. In (a), continuous vector – slab-derived fluids; dashed vector – sediment input in the source as represented and discussed by Woodhead *et al.* (2001). Bulk crust (BC) compositions are from Rudnick & Gao (2003). In (b), 'PM' denotes the values normalized to the primitive mantle; the fields of the subduction and carbonatite-related metasomatism are from La Flèche, Camiré & Jenner (1998). In (c), the fields for Hannuoba tholeiitic, transitional and alkalic basalts are after Zhi *et al.* (1990); the horizontal dashed line separates fields expected for melting garnet- and spinel-bearing peridotite as determined for the Cenozoic basalts in the Basin and Range province (Wang *et al.* 2002); 'N' denotes the values normalized to the chondrite.

https://doi.org/10.1017/S0016756810000373 Published online by Cambridge University Press

(3.9–5.5), Th/U (2.0–3.4), Th/Yb (1.6–4.0) and Lu/Hf (0.03–0.07) ratios to those of the average continental crust with La_N/Yb_N (8.2–11.7), Ce/Pb (2.9–4.4), Th/U (3.8–6.0), Th/Yb (0.8–4.9) and Lu/Hf (0.06–0.13) (Rudnick & Gao, 2003). Third, the presence of abundant *c.* 2.5 Ga inherited zircons in the dykes also indicates the involvement of ancient crustal components (Wu *et al.* 2006).

These geochemical attributes are generally regarded to be inherent in the melts either from an enriched mantle source that was formed by metasomatism of recycled crustal materials prior to magma generation or from a depleted mantle source that was contaminated by crustal material during magma ascent and emplacement. In our case, given the aforementioned consensus that the Mesozoic sub-continental lithospheric mantle beneath Western Liaoning is of EM-1 affinity with $\varepsilon_{Nd}(t) \approx -6.0$ and $(^{87}Sr/^{86}Sr)_i \approx 0.7060$, discernable higher $\varepsilon_{Nd}(t)$ values of the mafic dykes suggest that another end-member with more depleted isotopic compositions must have been involved in their formation. Therefore, we consider that this depleted end-member is most likely an asthenospheric derivative, as is the case with their possible analogues (Shao *et al.* 2006; Yang *et al.* 2007; Gao *et al.* 2008). Moreover, the relatively low $(La/Sm)_N$ (2.25–2.86) and $(Tb/Yb)_N$ (1.65–1.93), in combination with relatively flat MREE to HREE patterns for the mafic dykes, indicate that they may have been formed by a relatively high degree of partial melting of a mantle source in the spinel facies field and thus at depths shallower than 70 km (Fig. 7c).

To test this possibility, we adopted the assimilation–fractional–crystallization equation of DePaolo (1981) to model combined assimilation and fractional crystallization during magmatic differentiation. Given the intrusion of the mafic dykes into the deep-seated granitic batholith and their relatively low $^{87}Sr/^{86}Sr$ ratios, involvement of an upper crustal component seems to be insignificant. For the hosting Yiwulüshan granitic batholith including the Hengshan monzogranites, their peraluminous mineralogy, adakitic trace element signature, low initial $^{87}Sr/^{86}Sr$ ratios and strongly negative $\varepsilon_{Nd}(t)$ values (Fig. 6) argue for a felsic magma source that dominantly originated from partial melting of ancient meta-igneous lower crust, possibly in response to underplating of mafic mantle-derived magmas (Liu *et al.* 2002; Zhang *et al.* 2008*b*). Therefore, the two end-members chosen for the modelling are primitive melts from a depleted asthenospheric mantle (Zindler, Staudigel & Batiza, 1984) and melts from the Precambrian mafic lower crust. The latter is typified by Archaean granulite facies gneisses of the North China craton (Jahn *et al.* 1999). The adopted parameters are determined by referring to those used for other similar alkaline basaltic magma systems from the North China craton (ratio of assimilation to crystallization (r) of 0.2, D_{Sr} of 1.6, D_{Nd} of 1.2, e.g. Chen *et al.* 2008). As shown in Figure 6, the modelling results confirm that the mafic dykes could be generated by 12–15 % crustal contamination of the assumed parental magma coupled with significant fractional crystallization ($r = 0.2$).

6.b. Implication for lithospheric thinning

Continental mantle-derived mafic rocks of different ages from the same terrane are valuable archives for documenting secular chemical–thermal evolution of the deep continental lithosphere and underlying mantle. In the case of the Yanshan belt, the pioneering study on mantle xenoliths in several Palaeozoic kimberlite fields from Liaoning province documented a Palaeozoic lithosphere with an approximate thickness of 80–150 km (Menzies, Fan & Zheng, 1993), much greater than that of the present-day lithosphere beneath the Bohai Sea as revealed by geophysical evidence (Griffin *et al.* 1998). Late Triassic alkaline ultramafic rocks from northern Hebei province (Yan *et al.* 2000) exhibit a silica-undersaturated character, indicating their derivation from subtly metasomatized lithospheric mantle when the lithosphere was greater than 80 km thick, as constrained by experiments for silica-undersaturated alkaline basalts (Falloon *et al.* 1988; DePaolo & Daley, 2000). Early Jurassic flood basalts of the Nandaling Formation and Middle Jurassic basalts of the Lanqi Formation, with their moderately enriched isotopic signatures, argue for an origin from moderately refertilized lithospheric mantle with a thickness between 70 and 80 km (Wang *et al.* 2007; Yang & Li, 2008). Early Cretaceous basalts of the Yixian Formation, with their transitional signatures between lithosphere and asthenosphere (Yang & Li, 2008), may have formed when the lithosphere was between 65 and 80 km thick (DePaolo & Daley, 2000). Late Early Cretaceous basalts of the Zhanglaogongtun Formation possess MORB-like isotopic Sr–Nd–Pb signatures and thus have been derived from the asthenosphere when the lithosphere was less than 65 km thick (Zhang *et al.* 2003; Yang & Li, 2008).

With their respective origins from enriched lithospheric mantle and asthenosphere, the contrasting Middle Jurassic and Early Cretaceous mafic intrusive rocks presented herein are largely compatible with the lithospheric thinning trend beneath the Yanshan belt, as recorded by multiple episodes of Mesozoic mafic volcanic rocks from western Liaoning (Fig. 8). Together, they constitute an insightful magmatic proxy record for plumbing the depth of the lithosphere, and record a secular lithospheric evolution from an 80–150 km thick Palaeozoic refractory cratonic lithosphere through a 65 km thick late Mesozoic fertile lithosphere into an 80 km thick Cenozoic oceanic lithospheric mantle.

At present, various models have been proposed for the mechanism of the lithospheric thinning of the North China craton. Most representative ones include delamination (Gao *et al.* 2004), thermal-chemical erosion (Xu, 2001) or replacement (Zheng *et al.* 2001; Zhai *et al.* 2007), transformation through peridotite–melt interaction (Zhang *et al.* 2003, 2009;

https://doi.org/10.1017/S0016756810000373 Published online by Cambridge University Press

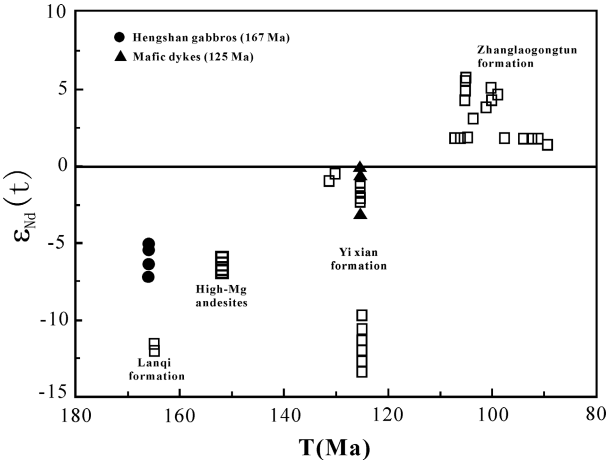

Figure 8. Variations of $\varepsilon_{Nd}(t)$ with time of the mafic rocks from western Liaoning. Data sources: Lanqi formation – Yang & Li (2008); Yixian formation – Shao *et al.* (2006); Gao *et al.* (2008), Yang & Li (2008); high-Mg andesite – Zhang *et al.* (2003); Zhanglaogongtun formation – Zhang *et al.* (2003); Yang & Li (2008).

Zhang, 2005, 2009), or hydro-weakening (Niu, 2005; Kusky, Windley & Zhai, 2007*b*). The strengths and weaknesses of these models have been widely discussed (Kusky, Windley & Zhai, 2007*b*; Menzies *et al.* 2007; Wu *et al.* 2008; Zhang *et al.* 2009; Zhang, 2007, 2009) and their scrutiny is beyond the scope of this paper. However, what is important to note is that this phenomenal lithospheric thinning is most likely not a consequence of any single thermal or mechanical event, but a combined result of peridotite–melt interaction, an enhanced regional thermal anomaly and lithospheric extension (Zhang, 2009). In this comprehensive mechanism, a precursory hydro-weakening or rock–fluid interaction is necessary for subsequent lithospheric thinning (Kusky, Windley & Zhai, 2007*b*; Zhang, 2009). Without this prerequisite stage, later lithospheric extension and regional thermal elevation could not trigger large-scale partial melting and lithospheric extension as observed in the North China craton. This is especially true for the Yanshan belt, where a fluid-dominated metasomatic character is widely observed in Mesozoic lithosphere-derived mafic rocks (this study and Fan *et al.* 2007; Guo *et al.* 2007; Zhang, 2007). The fluid-dominated metasomatism may have resulted in an amphibole- (or phlogopite-) bearing harzburgitic mantle (Wyllie & Sekine, 1982), which has a substantially lower solidus temperature than refractory lithospheric mantle and could be preferentially partially melted during the initial stages of thermal perturbation owing to extension.

6.c. Geodynamic implications

Recent general consensus is that the Mesozoic lithospheric thinning of the North China craton was not an isolated event, but a successive or multi-staged process that was closely related to the life cycles of the circum-cratonic orogenic belts (Fan *et al.* 2007; Guo *et al.* 2007; Yang & Li, 2008; Zhang, 2007, 2009; Zhang *et al.* 2009; Zhai *et al.* 2007). Therefore, any model that attributes this prolonged lithospheric thinning to a single event or geodynamic setting seems to contradict the nearly continuous magmatism on the North China craton, which lasted from 180 to 90 Ma.

For the generation of the isotopically enriched continental mafic magmas like those in the Mesozoic Yanshan belt, at least two essential steps are required: an earlier hydro-weakening stage that imparts subduction-related signatures to a precursor refractory lithospheric mantle, and a later stage of lithospheric extension and elevated thermal anomaly that induces asthenospheric upwelling and triggers partial melting of the refertilized lithosphere.

Such a two-stage scenario is coincident with the life cycle of the circum-cratonic orogenic belts of the North China craton. It has been a graveyard for oceanic lithospheres since early Palaeozoic time (e.g. Niu, 2005; Kusky, Windley & Zhai, 2007*a*,*b*), as recorded by ancient subduction zones responsible for consuming the early Palaeozoic–Permian Palaeo-Asian ocean (Xiao *et al.* 2003; Zhang *et al.* 2008*a*), the more northerly Mongol-Okhotsk ocean in the Jurassic (Tomurtogoo *et al.* 2005), and eastern Palaeo-Pacific oceanic crust from 200 to 100 Ma (Arakawa & Shinmura, 1995). These subduction zones probably contributed large quantities of water-rich fluids and melts into the sub-continental lithosphere and asthenosphere beneath the Yanshan belt, which would have led to significant hydration-related weakening of the lithosphere and formation of a heterogeneously modified lithospheric mantle.

As revealed by numerous studies on the Jurassic to Cretaceous mafic volcanic rocks (Zhang *et al.* 2003; Guo *et al.* 2007; Yang & Li, 2008), the Middle–Late Jurassic adakitic granitoids (Liu *et al.* 2002; Davis, 2003) and the Early Cretaceous alkaline plutons (Yang *et al.* 2008), Late Mesozoic magmatism in the Yanshan belt seems to experience a transition in character from an earlier, subduction-related calc-alkaline suite to a later continental intraplate-type alkaline suite. This trend is well documented by numerous post-collisional to within-plate magmatic associations worldwide (Coulon *et al.* 2002; Bonin, 2004; Duggen *et al.* 2005). In terms of crustal-level signature, the widespread occurrence of large-scale basin formation (Meng *et al.* 2003; Cope & Graham, 2007) and metamorphic core complexes (Davis *et al.* 2001, Zhang, Wang & Ma, 2003; Darby *et al.* 2004) in the Yanshan belt during Early Cretaceous time also attests to a prevalent intraplate extensional regime at the very end of the post-orogenic stage (Bonin, 2004). Consequently, we suggest that the Yanshan belt might be under a post-collisional/orogenic geodynamic setting associated with the northern Mongolo-Okhotsk suture during Middle–Late Jurassic to Early Cretaceous times.

Post-collisional/orogenic regimes are rife with thermal anomaly pulses and lithospheric extension (Liégeois, 1998). This may be driven by slab detachment or break-off (Davies & von Blankenburg,

https://doi.org/10.1017/S0016756810000373 Published online by Cambridge University Press

1995), gravitational collapse (Rey, Vanderhaeghe & Teyssier, 2001), delamination (Kay & Kay, 1993) and/or convective removal of the lithosphere (e.g. England & Houseman, 1989). All these processes cause upwelling of the asthenosphere that would perturb the original thermal gradient and lead to magma generation and lithospheric extension (Bonin, 2004).

As opposed to the short-term mechanisms like slab break-off or lithospheric delamination, gravitational collapse has been widely accepted to account for various extension and thinning processes of the previously thickened crust in orogenic belts during the protracted waning stages of their orogenic evolution (Rey, Vanderhaeghe & Teyssier, 2001; Vanderhaeghe & Teyssier, 2001). It is commonly induced by other thermal and mechanical triggers, such as (1) a sudden increase of gravitational potential energy related to asthenospheric upwelling either caused by convective removal or by delamination of the lithospheric mantle root, (2) a decrease in tectonic force applied at the boundary of the system related to a decrease in plate convergence, or (3) a decrease in the strength at the base of the zone of thickened crust due to thermal weakening (Vanderhaeghe & Teyssier, 2001). It often leads to the development of a broad low-strain extensional domain (rift basins) and localized high-strain extensional structures (such as metamorphic core complexes and associated plutonism), as in the case of Cenozoic North American Cordillera (Liu, 2001). Hence, it is clear that the model of gravitational collapse could be compatible with the prevalent upper crustal extensional architecture in the Yanshan belt during Early Cretaceous time. This is also consistent with the lack of post-rift subsidence in Cretaceous basins of the Yanshan belt, which is against wholesale lithospheric delamination but could be attributable to the mitigating effect of middle–lower crustal flow (Meng *et al.* 2003; Cope & Graham, 2007).

In conclusion, the Yiwulüshan case of western Liaoning province seems to present a specific example that internal-driven gravitational collapse, facilitated by thermal weakening of the lower crust due to protracted Late Mesozoic magmatism (*c*. 220–125 Ma), led to localized lithospheric thinning and the formation of upper crustal basin-and-range extensional structures during the waning stage of post-orogenic thermal and stress relaxation. It was not until the Cenozoic that the wholesale lithospheric thinning occurred in the Yanshan belt (Cope & Graham, 2007).

7. Conclusions

Zircon U–Pb dating and geochemical investigation documented two episodes of mafic intrusions in Yiwulüshan of western Liaoning from the Yanshan belt, North China craton: the Middle Jurassic hornblende gabbros and the Early Cretaceous mafic dykes. Geochemical and isotopic tracing suggest that the former were most likely derived from partial melting of subcontinental lithospheric mantle metasomatically enriched by fluids from earlier subduction processes, while the latter could be explained by lower crustal assimilation and fractional crystallization processes of mafic magmas derived from partial melting of a fertile asthenospheric mantle source in the spinel stability field. These two contrasting mafic intrusive suites, together with multiple Mesozoic mafic volcanic rocks from western Liaoning, provide an ideal magmatic proxy record for documenting the localized Mesozoic lithospheric thinning in the Yanshan belt, possibly triggered by gravitational collapse within an evolved post-collisional to within-plate extensional regime.

Acknowledgements. We gratefully acknowledge He Li and Xindi Jin for their help in major and trace element analyses, and Chaofeng Li for help in Sr–Nd isotope analyses. This study was financially supported by the National Natural Science Foundation of China (Grant nos 90914008 and 40873026), the Knowledge Innovation Program of the Chinese Academy of Sciences (Grant no. KZCX2-YW-QN115), and the Major State Basic Research Program of the People's Republic of China (Grant no. 2006CB403504). We are also grateful to Dr Mark Allen and two anonymous reviewers for their constructive suggestions that substantially improved the manuscript. This is The Institute for Geoscience Research (TIGeR) publication no. 222.

References

ARAKAWA, Y. & SHINMURA, T. 1995. Nd–Sr isotopic and geochemical characteristics of two contrasting types of calc-alkaline plutons in the Hida belt, Japan. *Chemical Geology* **124**, 217–32.

BONIN, B. 2004. Do coeval mafic and felsic magmas in post-collisional to within-plate regimes necessarily imply two contrasting mantle and crustal sources? A review. *Lithos* **78**, 1–24.

CHEN, B., TIAN, W., JAHN, B. M. & CHEN, Z. 2008. Zircon SHRIMP U–Pb ages and in-situ Hf isotopic analysis for the Mesozoic intrusions in South Taihang, North China craton: evidence for hybridization between mantle-derived magmas and crustal components. *Lithos* **102**, 118–37.

COPE, T. D. & GRAHAM, S. A. 2007. Upper crustal response to Mesozoic tectonism in western Liaoning, North China, and implications for lithospheric delamination. In *Mesozoic sub-continental lithospheric thinning under eastern Asia* (eds M. G. Zhai, B. F. Windley, T. M. Kusky & Q. R. Meng), pp. 201–22. Geological Society of London, Special Publication no. 280.

COULON, C., MEGARTSI, M., FOURCADE, S., MAURY, R., BELLON, H., LOUNI-HACINI, A., COTTON, J., COUTELLE, A. & HERMITTE, D. 2002. Post-collisioanal transition from calc-alkaline to alkaline volcanism during the Neogene in Oranie (Algeria): magmatic expression of a slab breakoff. *Lithos* **62**, 87–110.

DARBY, B. J., DAVIS, G. A., ZHANG, X. H., WU, F. Y., WILDE, S. A. & YANG, J. H. 2004. The newly discovered Waziyu metamorphic core complex, Yiwulüshan, western Liaoning province, North China. *Earth Science Frontiers* **11**, 145–55.

DAVIES, J. H. & VON BLANCKENBURG, F. 1995. Slab breakoff: a model of lithosphere detachment and its test in the magmatism and deformation of collisional orogens. *Earth and Planetary Science Letters* **129**, 85–102.

DAVIS, G. A. 2003. The Yanshan belt of North China: tectonics, adakitic magmatism, and crustal evolution. *Earth Science Frontiers* **10**, 373–84.

DAVIS, G. A., ZHENG, Y., WANG, C., DARBY, B. J., ZHANG, C. & GEHRELS, G. E. 2001. Mesozoic tectonic evolution of the Yanshan fold and thrust belt, with emphasis on Hebei and Liaoning provinces, northern China. In *Paleozoic and Mesozoic tectonic evolution of central and eastern Asia: From continental assembly to intracontinental deformation* (eds M. S. Hendrix & G. A. Davis), pp. 171–97. Geological Society of America, Memoir no. 194.

DEPAOLO, D. J. 1981. Trace element and isotopic effects of combined wallrock assimilation and fractional crystallization. *Earth and Planetary Science Letters* **53**, 189–202.

DEPAOLO, D. J. & DALEY, E. E. 2000. Neodymium isotope in basalts of the southwest basin and range and the lithospheric thinning during continental extension. *Chemical Geology* **169**, 157–85.

DUGGEN, S., HOERNLE, K., VAN DEN BOGAARD, P. & GARBE-SCHÖNBERG, D. 2005. Post-collisional transition from subduction- to intraplate-type magmatism in the westernmost Mediterranean: evidence for continental-edge delamination of subcontinental lithosphere. *Journal of Petrology* **46**, 1155–1201.

ENGLAND, P. & HOUSEMAN, G. 1989. Extension during continental convergence, with application to the Tibetan Plateau. *Journal of Geophysical Research* **94**, 17561–79.

FALLOON, T. J., GREEN, D. H., HARTON, C. J. & HARRIS, K. J. 1988. Anhydrous partial melting of a fertile and depleted peridotite from 2 to 30 kb and application to basalt petrogenesis. *Journal of Petrology* **29**, 1257–82.

FAN, W. M., GUO, F., WANG, Y. J. & ZHANG, H. F. 2007. Late Mesozoic mafic magmatism from the North China Block: constraints on chemical and isotopic heterogeneity of the subcontinental lithospheric mantle. In *Mesozoic sub-continental lithospheric thinning under eastern Asia* (eds M. G. Zhai, B. F. Windley, T. M. Kusky & Q. R. Meng), pp. 77–100. Geological Society of London, Special Publication no. 280.

FARMER, G. L. 2003. Continental basaltic rocks. Composition of the continental crust. In *The Crust, Treatise in Geochemistry*, vol. 3 (ed. R. L. Rudnick), pp. 85–121. Elsevier.

FOWLER, M. B. & HENNEY, P. J. 1996. Mixed Caledonian appinite magmas: implications for lamprophyre fractionation and high Ba–Sr granite genesis. *Contributions to Mineralogy and Petrology* **126**, 199–215.

FURMAN, T. & GRAHAM, D. 1999. Erosion of lithospheric mantle beneath the East African Rift system: geochemical evidence from the Kivu volcanic province. *Lithos* **48**, 237–62.

GAO, S., RUDNICK, R. L., XU, W. L., YUAN, H. L., LIU, Y. S., WALKER, R. L., PUCHTEL, I. S., LIU, X. M., HUANG, H., WANG, X. R. & YANG, J. 2008. Recycling deep cratonic lithosphere and generation of intraplate mgamatism in the North China Craton. *Earth and Planetary Science Letters* **270**, 41–53.

GAO, S., RUDNICK, R. L., YUAN, H. L., LIU, X. M., LIU, Y. S., XU, W. L., AYERS, J., WANG, X. C. & WANG, Q. H. 2004. Recycling lower continental crust in the North China craton. *Nature* **432**, 892–7.

GRIFFIN, W. L., ZHANG, A. D., O'REILLY, S. Y. & RYAN, C. G. 1998. Phanerozoic evolution of the lithosphere beneath the Sino-Korean Craton. In *Mantle Dynamics and plate Interactions in East Asia* (eds M. F. J. Flower, S. L. Chung, C. H. Lo & T. Y. Lee), pp. 107–26. American Geophysical Union, Geodynamics Series no. 27.

GUO, F., FAN, W. M., LI, X. Y. & LI, C. W. 2007. Geochemistry of Mesozoic mafic volcanic rocks from the Yanshan belt in the northern margin of the North China Block: relations with post-collisional lithospheric extension. In *Mesozoic sub-continental lithospheric thinning under eastern Asia* (eds M. G. Zhai, B. F. Windley, T. M. Kusky & Q. R. Meng), pp. 101–30. Geological Society of London, Special Publication no. 280.

HAWKESWORTH, C. J., GALLAGHER, K., HERGT, J. M. & MCDERMOTT, F. 1993. Mantle and slab contribution in arc magmas. *Annual Review Earth and Planetary Science* **21**, 175–204.

JAHN, B. M., WU, F., LO, C. H. & TSAI, C. H. 1999. Crust–mantle interaction induced by deep subduction of the continental crust: geochemical and Sr–Nd isotopic evidence from post-collisional mafic–ultramafic intrusions of the northern Dabie complex. *Chemical Geology* **157**, 119–46.

KAY, R. W. & KAY, M. S. 1993. Delamination and delamination magmatism. *Tectonophysics* **219**, 177–89.

KUSKY, T. M., WINDLEY, B. F. & ZHAI, M. G. 2007*a*. Tectonic evolution of the North China Block: from orogen to craton to orogen. In *Mesozoic sub-continental lithospheric thinning under eastern Asia* (eds M. G. Zhai, B. F. Windley, T. M. Kusky & Q. R. Meng), pp. 1–34. Geological Society of London, Special Publication no. 280.

KUSKY, T. M., WINDLEY, B. F. & ZHAI, M. G. 2007*b*. Lithospheric thinning in eastern Asia: constraints, evolution, tests of models. In *Mesozoic sub-continental lithospheric thinning under eastern Asia* (eds M. G. Zhai, B. F. Windley, T. M. Kusky & Q. R. Meng), pp. 331–43. Geological Society of London, Special Publication no. 280.

LA FLÈCHE, M. R., CAMIRÉ, E. G. & JENNER, G. A. 1998. Geochemistry of post-Acadian, Carboniferous continental intraplate basalts from the Maritimes Basins, Magdalen Islands, Québec, Canada. *Chemical Geology* **148**, 115–36.

LEAKE, B. E., WOOLLEY, A. R., ARPS, C. E. S., BIRCH, W. D., GILBERT, M. C., GRICE, J. D., HAWTHORNE, F. C., KATO, A., KISCH, H. J., KRIVOVICHEV, V. G., LINTHOUT, K., LAIRD, J., MANDARINO, J. A., MARESCH, W. V., NICKEL, E. H., ROCK, N. M. S., SCHUMACHER, J. C., SMITH, D. C., STEPHENSON, N. C. N., UNGARETTI, L., WHITTAKER, E. J. W. & YOUZHI, G. 1997. Nomenclature of amphiboles: report of the Subcommittee on Amphiboles of the International Mineralogical Association, Commission on New Minerals and Mineral Names. *American Mineralogist* **82**, 1019–37.

LE MAITRE, R. W. 2002. *Igneous rocks: A classification and Glossary of Terms*, 2nd edn. Cambridge: Cambridge University Press, 236 pp.

LIAONING BUREAU OF GEOLOGY AND MINERAL RESOURCES (LBGMR). 1998. *1:50000 scale regional geology of Fuxin and Badaohao, Liaoning Province* (in Chinese).

LIÉGEOIS, J. 1998. Preface – some words on the post-collisional magmatism. *Lithos* **45**, XV–XVII.

LIU, D., NUTMAN, A. P., COMPSTON, W., WU, J. & SHEN, Q. 1992. Remnants of ≥ 3800 Ma crust in the Chinese part of the Sino-Korean craton. *Geology* **20**, 339–42.

LIU, H. T., SUN, S. H., LIU, J. M. & ZHAI, M. G. 2002. The Mesozoic high-Sr granitoids in the northern marginal region of North China Craton: geochemistry and source region. *Acta Petrologica Sinica* **18**, 257–74.

LIU, M. 2001. Cenozoic extension and magmatism in the North American Cordillera: the role of gravitational collapse. *Tectonophysics* **342**, 407–33.

LUDWIG, K. 2001. *User manual for isoplot/EX (2.49).* Berkeley Geochronology Center Special Publication No. 1a. 55 pp.

LUGMAIR, G. W. & MARTI, K. 1978. Lunar initial $^{143}Nd/^{144}Nd$: differential evolution of the lunar crust and mantle. *Earth and Planetary Science Letters* **39**, 349–57.

LUO, Z. K., MIAO, L. C., GUAN, K., QIU, Y. M., MCNAUGHTON, N. J. & GROVES, D. I. 2001. SHRIMP U–Pb zircon ages of magmatic rocks in Paishanlou gold mine district, Fuxin, Liaoning province, China. *Geochimica* **30**, 483–90.

MCCULLOCH, M. T. & GAMBLE, J. A. 1991. Geochemical and geodynamical constraints on subduction zone magmatism. *Earth and Planetary Science Letters* **102**, 358–74.

MENG, Q., HU, J., JIN, J., ZHANG, Y. & XU, D. 2003. Tectonics of the late Mesozoic wide extensional basin system in the China–Mongolia border region. *Basin Research* **15**, 397–415.

MENG, Q. & ZHANG, G. 2000. Geological framework and tectonic evolution of Qinling orogen, central China. *Tectonophysics* **323**, 183–96.

MENZIES, M. A. 1987. Metasomatic and enrichment processes in lithospheric peridotites, an effect of asthenosphere–lithosphere interaction. In *Mantle Metasomatism* (eds M. A. Menzies & C. J. Hawkesworth), pp. 313–61. London: Academic Press.

MENZIES, M. A., FAN, W. & ZHANG, M. 1993. Palaeozoic and Cenozoic lithoprobes and the loss of >120 km of Archean lithosphere, Sino-Korean craton, China. In *Magmatic Processes and Plate Tectonics* (eds H. M. Prichard *et al.*), pp. 71–81. Geological Society of London, Special Publication no. 76.

MENZIES, M. A., XU, Y. G., ZHANG, H. F. & FAN, W. M. 2007. Integration of geology, geophysics and geochemistry: A key to understanding the North China craton. *Lithos* **96**, 1–21.

NIU, Y. L. 2005. Generation and evolution of basaltic magmas: some basic concepts and a new view on the origin of Mesozoic–Cenozoic basaltic volcanism in eastern China. *Geological Journal of China Universities* **11**, 9–46.

PATIÑO DOUCE, A. E. 1997. Generation of metaluminous A-type granites by low-pressure melting of calc-alkaline granitoids. *Geology* **25**, 743–6.

PATIÑO DOUCE, A. E. & BEARD, J. S. 1995. Dehydration-melting of biotite gneiss and quartz amphibolite from 3 to 15 kbar. *Journal of Petrology* **36**, 707–38.

PEARCE, J. A., KEMPTON, P. D., NOWELL, G. M. & NOBLE, S. R. 1999. Hf–Nd element and isotope perspective on the nature and provenance of mantle and subduction components in western Pacific arc-basin systems. *Journal of Petrology* **11**, 1579–1611.

PLATT, J. P. & ENGLAND, P. C. 1993. Convective removal of lithosphere beneath mountain belts: thermal and mechanical consequences. *American Journal of Science* **293**, 307–36.

REY, P., VANDERHAEGHE, O. & TEYSSIER, C. 2001. Gravitational collapse of the continental crust: definitions, regimes, mechanisms and modes. *Tectonophysics* **342**, 435–49.

ROBERTS, M. P., PIN, C., CLEMENS, J. D. & PAQUETTE, J. 2000. Petrogenesis of mafic to felsic plutonic rock associations: the calc-alkaline Quérigut complex, French Pyrenees. *Journal of Petrology* **41**, 809–44.

RUDNICK, R. L. & GAO, S. 2003. Composition of the continental crust. In *The Crust, Treatise in Geochemistry*, vol. 3 (ed. R. L. Rudnick), pp. 1–64. Elsevier.

ŞENGÖR, A. M. C., NATAL'IN, B. A. & BURTMAN, V. S. 1993. Evolution of the Altaid tectonic collage and Palaeozoic crustal growth in Eurasia. *Nature* **364**, 299–307.

SHAO, J. A., CHEN, F. K., LU, F. X. & ZHOU, X. H. 2006. Mesozoic pulsative upwelling diapirs of asthenosphere in west Liaoning province. *Journal of China University Geoscience* **31**, 807–16.

SISSON, T. W., GROVE, T. L. & COLEMAN, D. S. 1996. Hornblende gabbro sill complex at Onion Valley, California, and a mixing origin for the Sierra Nevada batholith. *Contributions to Mineralogy and Petrology* **126**, 81–108.

STEIGER, R. H. & JÄGER, E. 1977. Subcommission on geochronology, convention on the use of decay constants in geochronology and cosmochronology. *Earth and Planetary Science Letters* **36**, 359–62.

STERN, R. J. 2002. Subduction zones. *Reviews of Geophysics* **40**, 1012, doi: 10.1029/2001RG000108.

SUN, S.-S. & MCDONOUGH, W. F. 1989. Chemical and isotopic systematics of oceanic basalts: implications for mantle composition and processes. In *Magmatism in the Ocean Basins* (eds A. D. Saunders & M. J. Norry), pp. 313–45. Geological Society of London, Special Publication no. 42.

TOMURTOGOO, O., WINDLEY, B. F., KRÖNER, A., BADARCH, G. & LIU, D. 2005. Zircon age and occurrence of the Adaatsag ophiolite and Muron shear zone, central Mongolia: constraints on the evolution of the Mongol-Okhotsk ocean suture and orogen. *Journal of the Geological Society, London* **162**, 125–34.

TURNER, S., ARNAUD, N., LIU, J., ROGERS, N., HAWKESWORTH, C., HARRIS, N., KELLY, S., van CALSTEREN, P. & DENG, W. 1996. Post-collision, shoshonitic volcanism on the Tibetan Plateau: implications for convective thinning of the lithosphere and the source of ocean island basalts. *Journal of Petrology* **27**, 45–71.

TURNER, S. P., PLATT, J. P., GEORGE, R. M. M., KELLEY, S. P., PEARSON, D. G. & NOWELL, G. M. 1999. Magmatism associated with orogenic collapse of the Betic-Alboran Domian, SE Spain. *Journal of Petrology* **40**, 1011–36.

VANDERHAEGHE, O. & TEYSSIER, C. 2001. Partial melting and flow of orogens. *Tectonophysics* **342**, 451–72.

WANG, K., PLANK, T., WALKER, J. D. & SMITH, E. I. 2002. A mantle melting profile across the Basin and Range, SW USA. *Journal of Geophysical Research* **107**, doi: 10.1029/2001JB000209.

WANG, X. R., GAO, S., LIU, X. M., YUAN, H. L., HU, Z. C., ZHANG, H. & WANG, X. C. 2006. Geochemistry of high-Mg andesites from the early Cretaceous Yixian Formation, western Liaoning: implications for lower crustal delamination and Sr/Y variations. *Science in China* (D) **49**, 904–14.

WANG, Z. H., ZHAO, Y., ZOU, H. B., LI, W. P., LIU, X. W., WU, H., XU, G. & ZHANG, S. H. 2007. Petrogenesis of the Early Jurassic Nandaling flood basalts in the Yanshan belt, North China craton: A correlation between magmatic underplating and lithospheric thinning. *Lithos* **96**, 543–66.

WATSON, S. & MCKENZIE, D. 1991. Melt generation by plumes: A study of Hawaiian volcanism. *Journal of Petrology* **32**, 501–37.

WILLIAMS, I. S. 1998. U–Th–Pb geochronology by ion microprobe. In *Applications of microanalytical techniques to understanding mineralizing processes* (eds M. A.

McKibben, W. C. Shanks III & W. I. Ridley), pp. 1–35. *Reviews in Economic Geology* **7**.

WINDLEY, B. F., ALEXEIEV, D., XIAO, W. J., KRONER, A. & BADARCH, G. 2007. Tectonic models for accretion of the Central Asian Orogenic belt. *Journal of the Geological Society, London* **164**, 31–47.

WOODHEAD, J. D., HERGT, J. M., DAVIDSON, J. P. & EGGINS, S. M. 2001. Hafnium isotope evidence for 'conservative' element mobility during subduction zone processes. *Earth and Planetary Science Letters* **192**, 331–46.

WU, F. Y., YANG, J. H., ZHANG, Y. B. & LIU, X. M. 2006. Emplacement ages of the Mesozoic granites in southeastern part of the the Western Liaoning province. *Acta Petrologica Sinica* **22**, 315–25.

WU, F. Y., XU, Y. G., GAO, S. & ZHENG, J. P. 2008. Lithospheric thinning and destruction of the North China Craton. *Acta Petrologica Sinica* **24**, 1145–74.

WYLLIE, P. J. & SEKINE, T. 1982. The formation of mantle phlogopite in subduction zone hybridization. *Contributions to Mineralogy and Petrology* **79**, 375–80.

XIAO, W., WINDLEY, B. F., HAO, J. & ZHAI, M. 2003. Accretion leading to collision and the Permian Solonker suture, Inner Mongolia, China: Termination of the central Asian orogenic belt. *Tectonics* **22**, 1069, doi: 10.1029 /2002TC001484.

XU, Y. G. 2001. Thermo-tectonic destruction of the Archean lithospheric keel beneath the Sino-Korean Craton in China: evidence, timing and mechanism. *Physics and Chemistry of Earth (A)* **26**, 747–57.

YAN, G., MU, B., XU, B., HE, G., TAN, L., ZHAO, H. & HE, Z. H. 2000. Geochronology and isotopic features of Sr, Nd, and Pb of the Triassic alkali intrusions in the Yanshan–Yinshan regions. *Science in China* (D) **30**, 384–7.

YANG, W. & LI, S. G. 2008. Geochronology and geochemistry of the Mesozoic volcanic rocks in Western Liaoning: implications for lithospheric thinning of the North China craton. *Lithos* **120**, 88–117.

YANG, J. H., SUN, J. F., CHEN, F. K., WILDE, S. A. & WU, F. Y. 2007. Sources and petrogenesis of Late Triassic doleritic dykes in the Liaodong peninsula: implications for post-collisional lithosphere thinning of the Eastern North China Craton. *Journal of Petrology* **48**, 1973–97.

YANG, J. H., WU, F. Y., WILDE, S. A., CHEN, F. K., LIU, X. M. & XIE, L. W. 2008. Petrogenesis of an alkali syenites–granite–rhyolite suite in the Yanshan fold and thrust belt, eastern North China craton: geochronological, geochemical and Nd–Sr–Hf isotopic evidence for lithospheric thinning. *Journal of Petrology* **49**, 315–51.

YANG, Y. H., WU, F. Y., WILDE, S. A., LIU, X. M., ZHANG, Y. B., XIE, L. W. & YANG, J. H. 2009. *In situ* perovskite Sr–Nd isotopic constraints on the petrogenesis of the Ordovician Mengyin kimberlites in the North China craton. *Chemical Geology* **264**, 24–42.

ZHAI, M. G., FAN, Q. C., ZHANG, H. F., SUI, J. L. & SHAO, J. A. 2007. Lower crustal processes leading to Mesozoic lithospheric thinning beneath eastern North China: underplating, replacement and delamination. *Lithos* **96**, 36–54.

ZHANG, H. F. 2005. Transformation of lithospheric mantle through peridotite–melt reaction: a case of Sino-Korean craton. *Earth and Planetary Science Letters* **237**, 768–80.

ZHANG, H. F. 2007. Temporal and spatial distribution of Mesozoic mafic magmatism in the North China Craton and implications for secular lithospheric evolution. In *Mesozoic sub-continental lithospheric thinning under eastern Asia* (eds M. G. Zhai, B. F. Windley, T. M. Kusky & Q. R. Meng), pp. 35–54. Geological Society of London, Special Publication no. 280.

ZHANG, H. F. 2009. Peridotite–melt interaction: a key point for the destruction of cratonic lithosphere mantle. *Chinese Science Bulletin* **54**, 249–59.

ZHANG, H. F., SUN, M., ZHOU, X. H., ZHOU, M. F., FAN, W. M. & ZHENG, J. P. 2003. Secular evolution of the lithosphere beneath the eastern North China Craton: Evidence from Mesozoic basalts and high-Mg andesites. *Geochimica et Cosmochimica Acta* **67**, 4373–87.

ZHANG, H. F., GOLDSTEIN, S. L., ZHOU, X. H., SUN, M. & CAI, Y. 2009. Comprehensive refertilization of lithosphere mantle beneath the North China Craton: further Os–Sr–Nd isotopic evidence. *Journal of the Geological Society, London* **166**, 249–59.

ZHANG, X. H., WANG, H. & MA, Y. J. 2003. $^{40}Ar/^{39}Ar$ age constraints on two NNE-trending ductile shear zones from Yanshan orogen, North China Craton. *International Geology Review* **45**, 936–47.

ZHANG, X. H., LIU, Q., MA, Y. L. & WANG, H. 2005. Geology, fluid inclusions, isotope geochemistry, and geochronology of the Paishanlou shear zone-hosted gold deposit, North China craton. *Ore Geology Review* **26**, 325–48.

ZHANG, X. H., ZHANG, H. F., TANG, Y. J., WILDE, S. A. & HU, Z. C. 2008*a*. Geochemistry of Permian bimodal volcanic rocks from Central Inner Mongolia, North China: Implication for Tectonic setting and Phanerozoic continental growth in Central Asian Orogenic Belt. *Chemical Geology* **249**, 262–81.

ZHANG, X. H., MAO, Q., ZHANG, H. F. & WILDE, S. A. 2008*b*. A Jurassic peraluminous leucogranite from Yiwulüshan, western Liaoning, North China Craton: age, origin and tectonic significance. *Geological Magazine* **145**, 305–20.

ZHAO, G. C., WILDE, S. A., CAWOOD, P. A. & SUN, M. 2001. Archean blocks and their boundaries in the North China Craton: lithological, geochemical, structural and P–T path constraints and tectonic evolution. *Precambrian Research* **107**, 45–73.

ZHENG, J. P., O'REILLY, S. Y., GRIFFIN, W. L., LU, F. X., ZHANG, M. & PEARSON, N. J. 2001. Relict refractory mantle beneath the eastern North China block: significance for lithosphere evolution. *Lithos* **57**, 43–66.

ZHENG, J. P., GRIFFIN, W. L., O'REILLY, S. Y., LU, F. X., WANG, C. Y., ZHANG, M., WANG, F. Z. & LI, H. M. 2004. 3.6 Ga lower crust in central China: new evidence on the assembly of the North China craton. *Geology* **32**, 229–32.

ZHOU, X. H., ZHANG, G. H., YANG, J. H., CHEN, W. J. & SUN, M. 2001. Sr–Nd–Pb isotope mapping of late Mesozoic rocks across northern margin of North China block and implications to geodynamic processes. *Geochimica* **30**, 10–23.

ZHI, X., SONG, Y., FREY, F. A., FENG, J. & ZHAI, M. 1990. Geochemistry of Hannuoba basalts, eastern China: constraints on the origin of continental alkaline and theoleiitic basalt. *Chemical Geology* **88**, 1–33.

ZINDLER, A., STAUDIGEL, H. & BATIZA, R. 1984. Isotope and trace element geochemistry of young Pacific seamounts: implications for the scale of upper mantle heterogeneity. *Earth and Planetary Science Letters* **70**, 175–95.